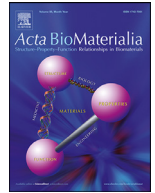




ELSEVIER

Contents lists available at ScienceDirect

Acta Biomaterialia

journal homepage: [www.elsevier.com/locate/actbio](http://www.elsevier.com/locate/actbio)

Full length article

## Living cells as a biological analog of optical tweezers – a non-invasive microrheology approach

William Hardiman<sup>a,\*</sup>, Matt Clark<sup>a</sup>, Claire Friel<sup>b</sup>, Alan Huett<sup>b</sup>, Fernando Pérez-Cota<sup>a</sup>, Kerry Setchfield<sup>a</sup>, Amanda J. Wright<sup>a,\*</sup>, Manlio Tassieri<sup>c</sup>

<sup>a</sup> Optics and Photonics Research Group, Faculty of Engineering, University of Nottingham, Glasgow, Nottingham NG7 2RD, UK

<sup>b</sup> School of Life Sciences, University of Nottingham, Medical School, QMC, Nottingham NG7 2UH, UK

<sup>c</sup> Division of Biomedical Engineering, James Watt School of Engineering, University of Glasgow, Glasgow, G12 8LT, UK

### ARTICLE INFO

#### Article history:

Received 22 December 2022

Revised 14 April 2023

Accepted 25 April 2023

Available online xxx

#### Keywords:

Passive microrheology

Cytoskeleton

Cellular biomechanics

Optical tweezers

### ABSTRACT

Microrheology, the study of fluids on micron length-scales, promises to reveal insights into cellular biology, including mechanical biomarkers of disease and the interplay between biomechanics and cellular function. Here a minimally-invasive passive microrheology technique is applied to individual living cells by chemically binding a bead to the surface of a cell, and observing the mean squared displacement of the bead at timescales ranging from milliseconds to 100s of seconds. Measurements are repeated over the course of hours, and presented alongside analysis to quantify changes in the cells' low-frequency elastic modulus,  $G'_0$ , and the cell's dynamics over the time window  $\sim 10^{-2}$  s to 10 s. An analogy to optical trapping allows verification of the invariant viscosity of HeLa S3 cells under control conditions and after cytoskeletal disruption. Stiffening of the cell is observed during cytoskeletal rearrangement in the control case, and cell softening when the actin cytoskeleton is disrupted by Latrunculin B. These data correlate with conventional understanding that integrin binding and recruitment triggers cytoskeletal rearrangement. This is, to our knowledge, the first time that cell stiffening has been measured during focal adhesion maturation, and the longest time over which such stiffening has been quantified by any means.

### Statement of significance

Here, we present an approach for studying mechanical properties of live cells without applying external forces or inserting tracers. Regulation of cellular biomechanics is crucial to healthy cell function. For the first time in literature, we can non-invasively and passively quantify cell mechanics during interactions with functionalised surface. Our method can monitor the maturation of adhesion sites on the surface of individual live cells without disrupting the cell mechanics by applying forces to the cell. We observe a stiffening response in cells over tens of minutes after a bead chemically binds. This stiffening reduces the deformation rate of the cytoskeleton, although the internal force generation increases. Our method has potential for applications to study mechanics during cell-surface and cell-vesicle interactions.

© 2023 The Authors. Published by Elsevier Ltd on behalf of Acta Materialia Inc.

This is an open access article under the CC BY license (<http://creativecommons.org/licenses/by/4.0/>)

## 1. Introduction

Single cell biomechanics is an area of increasing interest as changes in the mechanical properties of single cells have been linked to diseased and cancerous states of single cells [1–3]. However, a better understanding of the cytoskeleton's contributions

to the cells' biomechanic processes is still yearned by the scientific community. To fully explore the interplay between single cell biomechanics and the changing properties of the cytoskeleton, various measurement approaches are needed to observe these changes over long time courses with minimal perturbation to the living cell.

Many techniques are available to measure single cell biomechanics; some are measurements of whole cell deformation upon application of forces, whether by viscous drag [1], aspiration into micropipettes [4], or by optical forces [5]. Others, such as atomic force microscopy or Brillouin light scattering [6,7] can probe the

\* Corresponding authors.

E-mail addresses: [will.hardiman@nottingham.ac.uk](mailto:will.hardiman@nottingham.ac.uk) (W. Hardiman), [Amanda.Wright@Nottingham.ac.uk](mailto:Amanda.Wright@Nottingham.ac.uk) (A.J. Wright), [Manlio.Tassieri@Glasgow.ac.uk](mailto:Manlio.Tassieri@Glasgow.ac.uk) (M. Tassieri).

mechanical properties of cells with sub-micron resolution. Here we chemically affix micron-sized beads to the surface of living cells to monitor its dynamics over a long time period. This not only allows us to study the mechanical properties of cells on millisecond to second time-scales, but also the slow reorganization of their cytoskeleton on a much longer time-scale, all during the cells' natural interaction with a functionalised surface.

Analysis of cellular deformations requires a mechanical model of the cell [8–10], such as found in microrheology which is the study of fluid flow on micron length-scales. These scales enable study of microlitre samples too small for bulk rheology and at sub-millisecond time-scales. Microrheology techniques can be classified as either 'active', where an external force is applied to the sample, or 'passive', where the thermal energy acts as a driving force of probe particles. The simplest passive microrheology experiment, video particle tracking microrheology (VPTM), consists in recording videos of micron-sized particles suspended in the sample [11–13]. The trajectories of the tracer particles can be used to calculate the mean squared displacement (MSD) as a function of the time over which the displacement occurs, termed lag-time, or  $\tau$ . Under thermal equilibrium conditions, the generalised Stokes-Einstein relation can be used to relate the particles' MSD to either of the complex shear modulus  $G^*(\omega)$  [14], or to the shear creep compliance [15] of the suspending media.

The advantages of passive microrheology are twofold. Firstly, the full frequency spectrum of the complex modulus can be calculated from a single video recording; secondly the strain (or deformation) is smaller. The second advantage is especially apparent when probing living cells as they respond to applied forces, a process known as mechanotransduction. For example, cells have been seen to temporarily soften after deformations greater than 100nm lasting a few seconds [17,18]. Previous studies of integrin mechanics have focused on the viscoelastic properties of the integrin binding without consideration of either how the applied forces affect the mechanics of the cell, nor how cells' mechanics may change over many minutes [17,19]. Here, our passive approach allows us to probe the mechanics of the binding site as it evolves over an hour or more without perturbing the cells with external forces.

In this work, we demonstrate non-invasive passive microrheology of living cells to probe both thermal strain fluctuations at millisecond to second timescales and cytoskeletal remodeling over longer times, without mechanically disrupting the cells. Previous methods probing cellular mechanics have either been invasive [16], without probing their mechanics at short time-scales [20–22], or relied on application of external forces [23,24].

The proposed experimental method, consists on chemically affix a functionalised microsphere to the surface of a living cell, and to monitor its *pseudo*-Brownian motion with repeat measurements over multiple hours. The method was inspired by a previous work of Warren et al. [25], who first presented the experimental technique and a related "non-quantitative" analytical model. In this work, we have developed a framework for quantifying changes of the cells' rheological properties and analogous to microrheology with optical tweezers whereby the spatial confinement of the bead motion due to binding to the cell is analogous to that of an optical trap. This approach allows us (i) to quantify the viscosity of cells and to measure their cytoskeletal rearrangement, and importantly (ii) to discriminate between the change in cytoskeletal activity due to either of the cell stiffening or softening processes.

## 2. Analytical framework: Cells as a biological analog of optical tweezers

Warren et al. [25] adopted the theoretical framework introduced by Tassieri et al. [26] to interpret the *pseudo* Brownian motion of a bead (of radius  $R$ ) chemically attached onto the surface

of a cell and no longer optically trapped. The framework is described in brief here and in detail in Supplement A. In this case, the cell acts as a biological analog of Optical Tweezers and a possible generalised Langevin equation describing the forces acting on the bead was formulated:

$$m\ddot{a}(t) = \vec{f}_R(t) - \int_0^t [\zeta_c(t - \tau) + \zeta_s(t - \tau)]\vec{v}(\tau)d\tau, \quad (1)$$

where  $m$  is the mass of the particle,  $\ddot{a}(t)$  is its acceleration,  $\vec{v}(t)$  is its velocity,  $\vec{f}_R(t)$  is the resultant of all stochastic thermal forces acting on the particle. The integral term represents the total damping force acting on the bead, which (based on the superposition principle) incorporates two generalised time-dependent memory functions  $\zeta_c(t)$  and  $\zeta_s(t)$  that are representative of the viscoelastic nature of the cell and the solvent, respectively. In particular the above two memory functions are related to the frequency ( $\omega$ ) dependent complex shear modulus of the solvent and the cell by means of the following two expressions:  $G_c^*(\omega) \cong i\omega\hat{\zeta}_c(\omega)/6\pi a$  and  $G_s^*(\omega) = i\omega\hat{\zeta}_s(\omega)/\beta$ , respectively; where  $\hat{\zeta}_s(\omega)$  and  $\hat{\zeta}_c(\omega)$  are the Fourier transforms ("^") of  $\zeta_s(t)$  and  $\zeta_c(t)$ , and  $\beta$  is a constant of proportionality with dimensions of length introduced by Warren et al. [25] and assumed to be invariant for each cell-bead pair.  $\beta$  may vary for different cells as it depends on (i) the cell radius, (ii) the number and the dynamics of the chemical bonds between the bead and the cell, (iii) the contact area between the cell and the glass coverslip, and (iv) the relative position of the bead with respect to both the cell's equatorial plane and the glass coverslip.

By assuming the system to be at thermodynamic equilibrium, Eq. (1) can be solved for the viscoelastic modulus of the cell in terms of the Fourier transform of the normalised mean square displacement (NMSD,  $\Pi(\tau) = MSD(\tau)/MSD_p$  where  $MSD_p$  is the plateau MSD) of the bead [25]:

$$\frac{G_c^*(\omega)}{G_0} = \frac{1}{i\omega\hat{\Pi}(\omega)} + \frac{m\omega^2}{\beta G_0} - \frac{6\pi R G_s^*(\omega)}{\beta G_0}, \quad (2)$$

where  $\beta G_0 = k_B T / \langle r^2 \rangle$ , is the limiting value, for vanishingly low frequencies, of the real part of the complex modulus of the compound system (i.e. cell plus solvent), which in this work is  $\beta G_0 \cong G_c^*(\omega)$  for  $\omega \rightarrow 0$ .  $k_B$  is the Boltzmann constant,  $T$  is the absolute temperature and  $\langle r^2 \rangle$  is the variance of the particle's trajectory. In order to simplify Eq. (2) we make the following two assumptions: (i) for micron-sized polystyrene beads, the inertia term  $m\omega^2$  is negligible up to frequencies on the order of MHz and (ii) for solvents having frequency-independent viscosity  $\eta_s$  (e.g., water),  $G_s^*(\omega)$  simplifies to  $i\omega\eta_s$  and the last term in Eq. (2) becomes negligible for the range of frequencies explored in this work (even with Faxn's correction to the apparent viscosity due to the proximity to the glass surface). Thus, Eq. (2) can be further simplified into:

$$\frac{G_c^*(\omega)}{G_0} \cong \frac{1}{i\omega\hat{\Pi}(\omega)}, \quad (3)$$

which provides a means of measuring the viscoelastic properties of the cell (scaled by  $G_0$ ) over a range of frequencies. In practice the frequency range is limited at high frequencies by the acquisition rate of the detector used for tracking the bead position, and at low frequencies by cytoskeletal reorganisations driving bead motion of greater magnitudes than the thermal motion.

## 3. Microrheology experiments

### 3.1. Data collection

Polystyrene beads of 5 $\mu$ m diameter, functionalised with streptavidin (Spherotech, USA) to facilitate binding to the cell, are added to the media once a cell is chosen for imaging. The beads take a couple of minutes to sediment to the bottom of the sample holder,

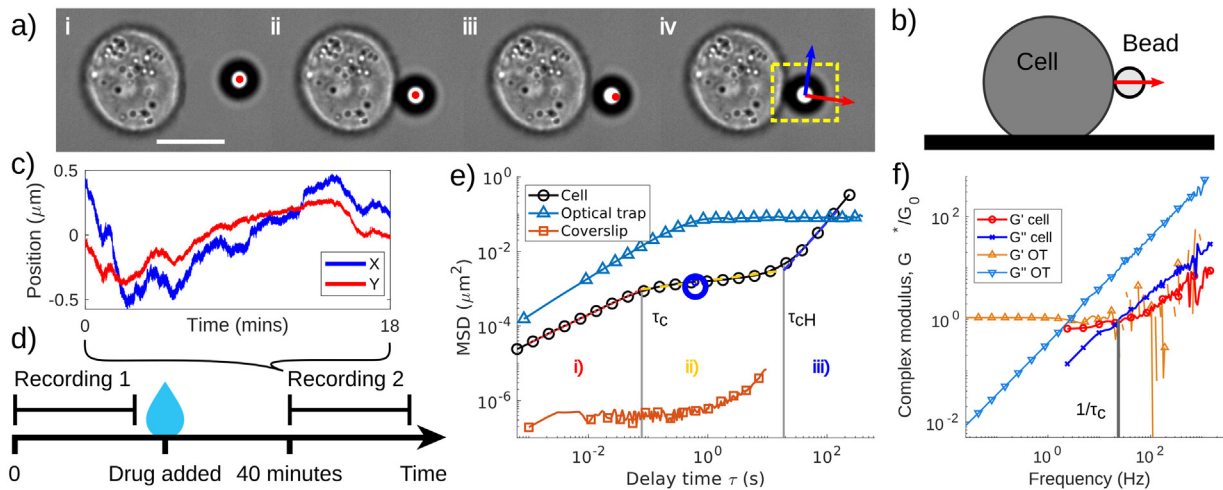


**Fig. 1.** Data collection and interpretation. a) Experimental procedure as described in text. Red and blue arrows denote radial and tangential directions, respectively. Yellow box shows region of interest. Scale bar in i is 10  $\mu\text{m}$ . b) Schematic side view of bead attached to cell. c) Position-time trace from 1 measurement; the 18 min trace consists of 2,000,000 observations. d) Experimental paradigm for change over time: two video measurements are taken 40 min apart with a drug being added after the first measurement, note that other measurements may have been made in this window, but only two are compared. e) log-log plot with three example MSD curves: typical data from bead attached to cell, optically trapped bead, and bead attached to coverslip (to demonstrate noise floor). Three regions are highlighted for the cell MSD: i) viscoelastic response at short time, ii) soft glassy plateau at intermediate time with power-law exponent minima indicated by blue circle, and iii) superdiffusion at long times. f) Normalised complex modulus of a cell (Eq. (3)), and of optical tweezers, calculated from the Fourier transform of the normalised MSD. Characteristic time scales found empirically are labelled on e) and f). (For interpretation of the references to color in this figure legend, the reader is referred to the web version of this article.)

then one is optically trapped (Fig. 1a i, red dot shows optical trap position). The trapped bead is brought to the edge of the cell and the focus control on the microscope is used to adjust the position in  $z$  relative to the cell with the ideal position shown in Fig. 1b. The cell is then brought into contact with the bead (Fig. 1a ii), judged by observing the bead displacing from the centre of the trap on contact with the cell. If the bead moves in  $z$  as contact is made then the focal position was incorrect, and the cell is moved away to adjust the  $z$  position of the bead. Motion of the bead in  $z$  is estimated by a change in the appearance (or brightness profile) of the bead.

Once the trapped bead is in contact with the cell, the laser power is reduced to form a weak trap ( $\kappa \sim 2 \mu\text{N}/\text{pm}$ ), which is used to attempt to remove the bead from the cell (Fig. 1a iii). The trap must be sufficiently weak to avoid pulling a membrane tether [27]. If the weak trap is unable to separate the bead from the cell, binding is confirmed, the trapping laser is turned off, and a small region of interest containing just the bead is imaged, as shown by yellow box in Fig. 1a iv. Videos recording the motion of the bead, typically comprising 1 million frames, are analysed by thresholding and centroiding to produce position-time tracks of the beads, an example of which can be seen in Fig. 1c.

During experiments, measurements were taken at regular intervals and, in order to better discriminate mechanical changes in the cell over time, two of these measurements roughly 40 min apart were chosen to be analysed (Fig. 1d). Drug treated cells had Latrunculin B added to the cell media dissolved in 200  $\mu\text{L}$  of DMEM at 2mM (the same volume as the media already in the microslide chamber), thus ensuring homogeneity of the drug concentration within the sample.

### 3.2. Data analysis

Offline data analysis was performed using MATLAB (Mathworks, USA). The videos were processed to extract the  $(x, y)$  coordinates of the bead position within each frame. The Cartesian coordinate were then transformed into polar coordinates  $(r, \theta)$  to separate the motion components into the radial and tangential directions,

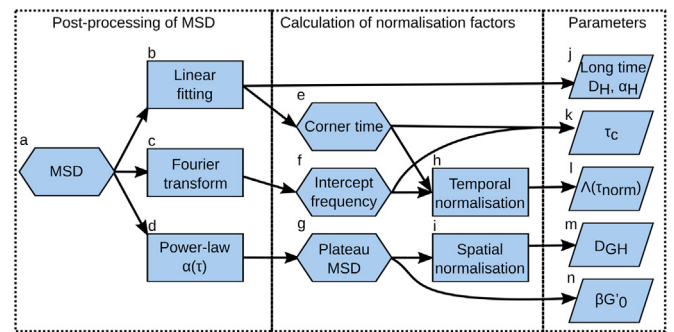


**Fig. 2.** Post-processing steps applied to experimental MSD data resulting in calculation of the 9 parameters listed on the right. Hexagons indicate values used during processing, rectangles indicate processing steps, rhomboids indicate the end-point measures, and arrows indicate flow of data between the steps. Each processing step and the interpretation of the parameters is explained in detail in the main text.

which are perpendicular and tangential to the cell surface, respectively. Notice that the tangential coordinate used for the analysis is defined as  $\vec{r} \cdot \vec{\theta}$ ; therefore, both coordinates have dimensions of length.

The MSD (see example in Fig. 1e) has been calculated using code adapted from that presented by Tarantino [28]. In particular, the original MATLAB code was modified to calculate the MSD not at all possible delay times (i.e., at lag times linearly spaced in time), but at lag-times logarithmically spaced in time, to reduce the overall processing time. The MSD was then analysed as schematically shown in Fig. 2. In order to evaluate the Fourier transform of experimental raw data (Fig. 2 box c), a numerical method was implemented in MATLAB based on the work of Evans et al. [29]. The recommendations of Tassieri and Smith were followed to reduce numerical errors at high frequencies [26,30].

#### 3.2.1. Stiffness and viscosity

We now explain our interpretation/analysis of the experimental MSD curves, starting from the low-frequency limit elastic modu-

lus of the cell  $\beta G'_0$ , which is analogue to the stiffness of an optical tweezers. Note that the latter can be easily calibrated by appealing to the principle of equipartition of energy for which only the variance of the bead position is needed [31]. In the case of optical tweezers, as long as any experimental drift has been corrected for then the variance of the bead position is equal to half the plateau value of the MSD at long lag-times [32]. Similarly, when a bead is bound to the surface of a cell, the bead's *pseudo*-diffusion is constrained by the binding on timescales of the order of a few seconds. Cells, however, do not remain stationary, and the dynamics of the attached bead are governed by the cytoskeletal reorganisation over timescales longer than a second, especially when beads are bound to integrin receptors of living cells [20,21,33]. As such, the variance ( $\langle r^2 \rangle$ ) of the bead position does not reflect the low-frequency limit of the cells' elastic modulus (as for the OT). Therefore, we have considered instead the half value of the plateau of the mean square displacement curve as a means of measuring the elastic plateau modulus of cells:

$$\beta G'_0 = \frac{2k_B T}{MSD_p}, \quad (4)$$

where  $MSD_p$  is the plateau value of the MSD that can be identified (Fig. 2 boxes d and g, shown in Fig. 1e circled in blue) as the MSD value at which the power-law exponent is minimum.

Another relevant parameter to be considered is the onset time of the MSD plateau, which in the case of an OT is given as  $t^* = (6\pi R\eta_s)/\kappa$ , where  $\kappa = 2k_B T/MSD_p$ , and  $\eta_s$  is the fluid dynamic viscosity (see Supplement A for more detail). Similarly, for a bead bound to a cell, we propose the following expression to evaluate the cell's dynamic viscosity:

$$\eta_c = \frac{\beta G'_0 \tau_c}{6\pi R} \equiv \eta_r \eta_s, \quad (5)$$

which can be determined by using the geometric stiffness,  $\beta G'_0$ , as defined in Eq. (4), and the corner time  $\tau_c$ , measured experimentally. In Eq. (5)  $\eta_r = \eta_c/\eta_s$  is the relative viscosity of the cell, and is valid for times up to the characteristic relaxation time. In order to determine  $\tau_c$  from the MSD data, two methods were adopted either in the time or in the frequency domain and a normalisation was performed by using the mean value of these times. In the time domain (Fig. 2 boxes b and e, labelled  $\tau_c$  on Fig. 1e), the corner times are estimated by the abscissa value of the intercept between the least-squares linear fits of the MSD data (drawn in a log-log plot) within the linear regions. In the frequency domain (Fig. 2 boxes c and f, shown in Fig. 1f as  $1/\tau_c$ ), the corner time is estimated by the inverse of the frequency for which  $\tan(\delta) = G''/G' = 1$ ; this is estimated by means of a least-squares fit of  $\log(\omega)$  against  $\log(\tan(\delta))$ .

### 3.2.2. Spatio-temporal normalisation

The identification of different characteristic timescales relevant to the cell-bead system allows time-domain normalisation. This has previously been demonstrated for optical trapping microrheology measurements [26], where it can remove variation due to different trap stiffness or sample viscous response. In the case of live cell microrheology, using normalisations allows us to pool data from different cells or to remove the effect that changing one parameter has on another, e.g.: change in cytoskeletal reorganisation independent of stiffening of cell. For both applications, the corner times and plateau MSDs are found empirically as described above (Fig. 2 boxes e, f, and g). The spatial normalisation is performed by dividing the MSD values by the plateau MSD, and the temporal normalisation by dividing the lag times by corner times. This allows better understanding of cytoskeletal reorganisation and increment distributions.

### 3.2.3. Cytoskeletal reorganisation

At long lag times, the bead undergoes super-diffusive motion (labelled as “iii” in Fig. 1e), brought about by active strain fluctuations within the cell due to cytoskeletal reorganisation. This is parameterised by means of least-squares linear fits of a portion of the experimental data to

$$\log(MSD) = \log(2D_H) + \alpha_H \log(\tau), \quad (6)$$

providing  $D_H$ , the pseudo-diffusion coefficient, and  $\alpha_H$ , the power-law exponent, as represented by Fig. 2, box j.  $D_H$  can be interpreted equivalently to rate of strain, or the square of the distance that the bead binding site moves in a given time. At long lag-times,  $1 < \alpha_H < 2$ , ruling out both thermal motion (which has a power-law exponent  $\leq 1$ ) and experimental drift (which has power-law exponent = 2) as the source of the superdiffuse motion.

### 3.2.4. Increment distributions

In order to better understand the driving forces behind bead motion, we have examined the normalised increment distribution as a function of lag time,

$$z(\tau) = \frac{\Delta r - \overline{\Delta r}}{STD(\Delta r)} \Big|_{\tau}, \quad (7)$$

where  $\Delta r(\tau) = r(t + \tau) - r(t)$  is the increment series for a given lag-time ( $\tau$ ),  $\overline{\Delta r}$  is its mean and  $STD(\Delta r_\tau)$  is its standard deviation. Notice that, for Brownian motion, the increments are normally distributed across all time scales, as corroborated by our measurements performed with optical tweezers and shown later in Fig. 5. This prediction can be validated by considering the bead as an overdamped oscillator (Eq. (1)), in which the mean driving force is proportional to the displacement over a given time interval. If molecular motors have a significant driving contribution to motion, it is expected that the increment distribution will instead have a broad-tailed distribution [20].

To pool data from different cells, we first calculated the increment distribution for each cell as a function of lag-time, then time-domain normalisation was performed (Fig. 2 boxes h and i), and the increment distributions were added together before further analysis. The increment distributions were quantified using a non-Gaussian parameter [20,34],

$$\Lambda(\tau) = \frac{\langle z(\tau)^4 \rangle}{3\langle z(\tau)^2 \rangle^2} - 1, \quad (8)$$

where  $z(\tau)$  is the normalised increment distribution defined above. This approach quantifies the deviation from a normal distribution, with values  $\Lambda(\tau) > 0$  indicating a broad-tailed distribution.

## 4. Results

First we consider the effect of Latrunculin B on HeLa S3 cells visualised by means of confocal microscopy, as shown in Fig. 3. Latrunculin B is known to disrupt the actin filaments in the cytoskeleton. Several changes to cell morphology are visible after drug treatment: there are blebs present on many of the cells visible in Fig. 3e, the actin cortex is thinner and has fewer fibrous protrusions, the cell is less spread with less contact to the coverslip, and there is lower actin density where the cell contacts the substrate (Fig. 3d vs h). Also, after drug treatment, the nucleus appears to be further from the coverslip (Fig. 3c vs g), which may be caused by the reduced tension within the actin cytoskeleton.

Microrheology experiments were performed on control and drug treated HeLa S3 cells and the time-dependent behaviour of the MSD curves was inspected. For measurements where  $MSD|_{\tau=1s} < 10^{-4} \mu\text{m}^2$ , data was deemed to be too close to the noise floor (as shown by bead attached to coverslip in Fig. 1)

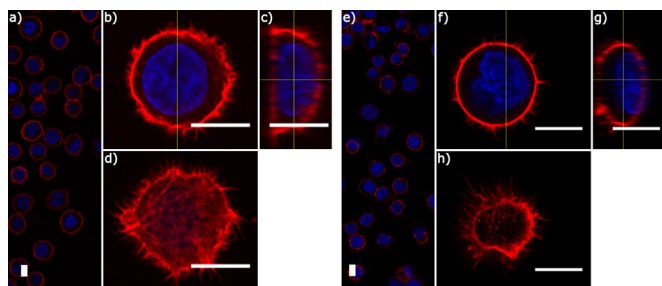


**Fig. 3.** Airy scan confocal images of actin cytoskeleton (red, phalloidin) and nucleus (blue, Hoescht 33342) in fixed HeLa S3 cells (a–d) and 10 min after Latrunculin B treatment to demonstrate the effect of the drug (e–h). (a, e) wide field of view, (b, f) medial plane with indicator of location of profile slice, (c, g) profile slice with indicator to show height of medial plane, and (d, h) basal plane. All scale bars are 10  $\mu$ m. (For interpretation of the references to color in this figure legend, the reader is referred to the web version of this article.)

meaning particle tracking would not be reliable and the data was therefore discarded. From looking at transmission images recorded of the cell-bead pair it is clear that in this discarded data set the beads had been partially engulfed by the cells. After purging these measurements, there remained data from 21 cells, 10 of which received drug treatment.

The MSD curves were interpreted and endpoint measures were calculated (Fig. 2) for two video recordings 40 min apart; when “change over 40 min” is used herein, it refers to the difference between the values at these two time stamps. Results are compared for drug treated and control conditions, and a Mann-Whitney  $u$ -test is used to determine whether the medians are significantly different. The  $u$ -test is performed using MATLAB’s *ranksum* function, where the data under drug treated and control conditions are used as the two inputs.

#### 4.1. The viscosity and elasticity of the cells

Consider now the viscoelastic shear properties of cells at timescales up to 1 s. The change over 40 min of the geometric stiffness,  $\beta G'_0$ , of the bead-cell system (Eq. (4), Fig. 2 box n) is shown in Fig. 4a, with the two perpendicular directions of motion analysed separately (radial and tangential directions identified by the red and blue symbols, respectively). From Fig. 4a it can be seen that during the 40 min experimental window the control cells stiffened, while the Latrunculin B treated cells softened. The tangential direction exhibited much smaller changes than the radial direction but showed the same trend. The distribution of stiffness changes for control and drug treated were found to be significantly different using a Mann-Whitney  $u$ -test ( $p < 0.01$ ). Notably, in analogy to OT measurements, where an increase in trap stiffness causes a decrease in plateau onset time (Eq. (5), Fig. 2 box k), the same behaviour is observed in the case of cells confirming that the control cells are stiffening over time whereas the drug treated cells are softening, as shown in Fig. 4b, with statistical significance ( $p < 0.05$ ).

This observation is further corroborated by the results shown in Fig. 4c–f, where data is pooled together into two categories: “no drug” (con) and “drug” (lat) (no drug: 33 measurements from 23 cells; drug: 50 measurements from 10 cells), and the inverse of the corner time is plotted against the geometric stiffness of the cells. The ordinate axis has been multiplied by the viscosity value of water ( $\eta_{\text{water}} = 1\text{mPa s}$ ) and the abscissa axis has been scaled by a geometrical factor related to the bead radius ( $6\pi r$ ), so that both the axis had the same dimensions and better represent Eq. (5). A visual inspection of Fig. 4c–f reveals that all cells have roughly equal and time-invariant viscosity as all measurements lay (over two decades) close to a single line of gradient 1 in a double logarithm plot (grey dotted line).

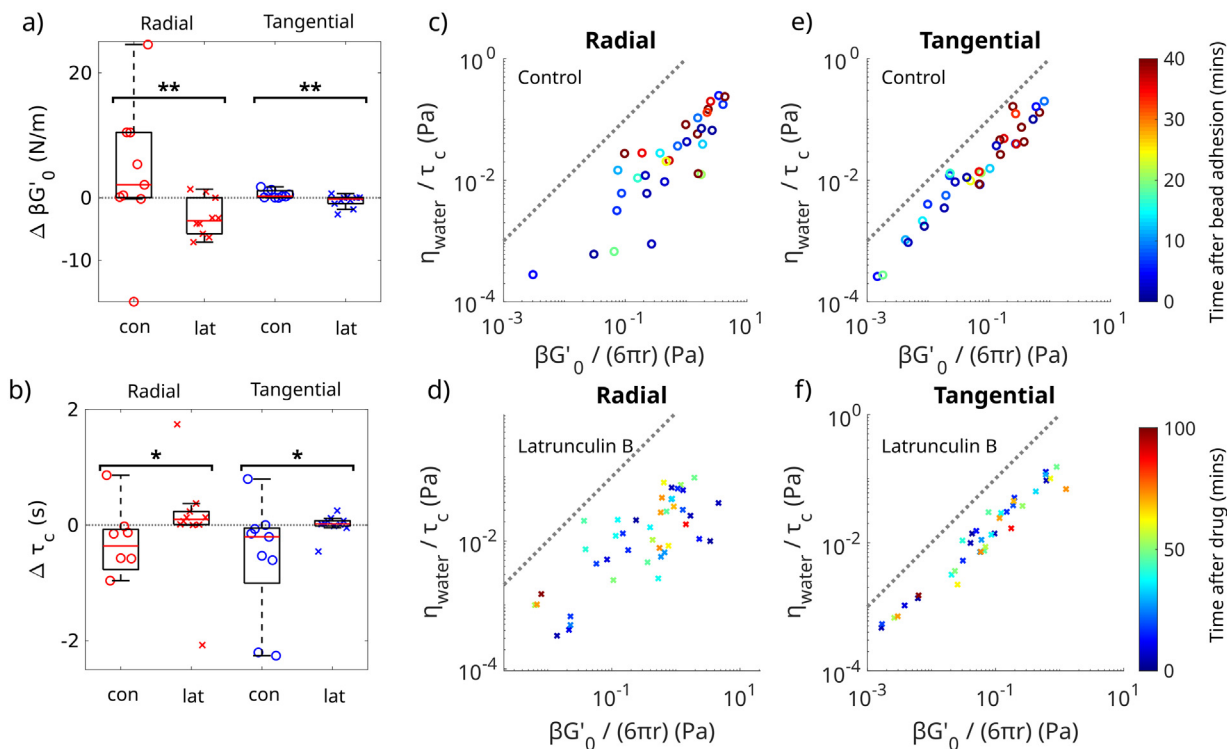


**Fig. 4.** Master curves demonstrating constant viscosity across all cell measurements. (a,b) Change in geometric stiffness (eq. 4) and plateau onset time (Eq. (5)), respectively, for control (con, circles) vs drug treated (lat, crosses) in radial (red) and tangential (blue) directions, respectively. \*\* denotes  $p < 0.01$  and \* denotes  $p < 0.05$  with Mann-Whitney  $u$ -test. (c–f) Master curves of plateau onset time scaled by viscosity of water against geometric stiffness scaled by bead radius, for control (c,e) and drug treated (d,f). Dashed lines are a guide showing prediction for an optically trapped bead in water. (For interpretation of the references to color in this figure legend, the reader is referred to the web version of this article.)

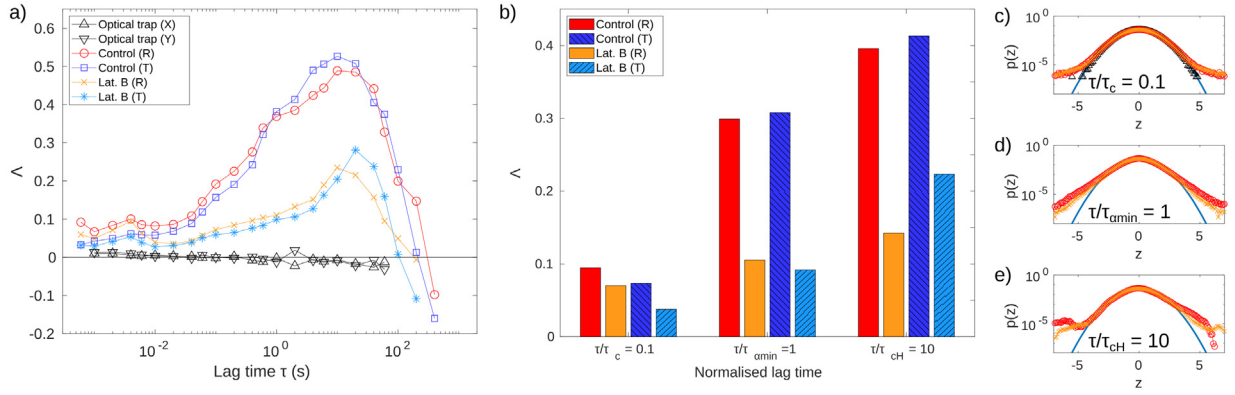


**Fig. 5.** a) Non-gaussian parameter  $\Delta(\tau)$  as a function of lag-time,  $\tau$ , for all control cells (33 measurements from 23 cells), all actin-disrupted cells (50 measurements from 10 cells), and an optically trapped bead in water. b) Non-gaussian parameter  $\Delta(\tau)$  at three different timescales: one-tenth of the plateau onset time  $\tau_c$ , the plateau minima time  $\tau_{amin}$ , and ten times the superdiffuse motion onset time  $\tau_{CH}$ . c-e) Radial increment distributions for each time scale - tangential distributions show the same behaviour and have been excluded to improve visual clarity.

Notice that the colour gradient of the markers in Fig. 4c-f relates to the time passed after the bead adhesion, and in the case of the results shown in Fig. 4c-e highlights the stiffening over the time of cells without drug treatment. Moreover, by fitting the data shown in Fig. 4c-e to

$$\log(\beta G'_0/6\pi r) = \log(\eta_{water}/\tau_c) + \log(\eta_r). \quad (9)$$

we quantify the viscosity probed independently of changes in power-law rheology or elastic stiffness. We found this viscosity for all cells in the radial direction to be  $23 \times \eta_{water}$  and in the tangential direction to be  $4 \times \eta_{water}$ . Furthermore, we found that Latrunculin B treatment does not affect the viscosity probed.

#### 4.2. Non-equilibrium behaviour

The increment distribution and non-Gaussian parameter (Eq. (8)) were calculated and data pooled into control and latrunculin B treated (actin-disrupted). Temporal normalisations were performed after calculating increment distributions but before data pooling. In Fig. 5a we report the non-Gaussian parameter for each of the above cases in both radial and tangential directions, along with the case of an optically trapped bead for comparison. It can be seen that the increment distributions are increasingly broad-tailed at long lag-times (larger value of non-Gaussian parameter) and more so for the control case than actin-disrupted.

In order to better understand the three characteristic regions of the MSD curve, three different characteristic regions were chosen for consideration: (i) one-tenth of the plateau onset time,  $\tau_c$ , is chosen as representative of short time dynamics (Fig. 5c); (ii) the time coincident with the power-law exponent minimum as representative of the glassy rheology of the cytoskeleton (Fig. 5d); and (iii) ten times the superdiffuse onset time,  $\tau_{CH}$ , as representative of the superdiffuse motion (Fig. 5e).

Normalisation of the delay time before accumulating the increment distributions allows characteristic times to be aligned, and the mean increment distributions to be inspected relative to these characteristic times. In Fig. 5b it can be seen that the broad-tailed increment distribution characteristic of non-equilibrium behaviour is coincident with the glassy plateau in the cell rheology (as seen on the MSD curve). While at shorter times, the bead motion is closer to equilibrium, with low values of  $\Delta(\tau)$  for all  $\tau/\tau_{amin} < 1$ , thus indicating that the bead motion is driven by a single Gaussian process.

Examination of the increment distributions at short lag-times reveal a distribution close to Gaussian, with little difference between control and actin-disrupted cells. For both, the increment

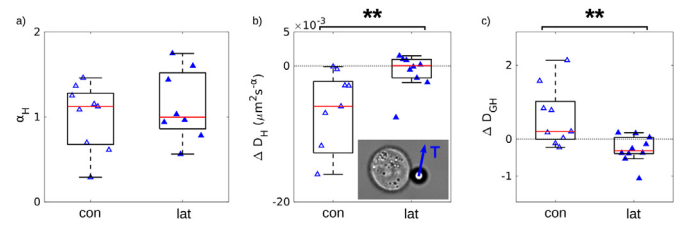


**Fig. 6.** Pseudo-diffusion parameters  $\alpha_H$  and  $D_H$  (Eq. (6)) for long time dynamics in tangential direction. a) Long time motion of beads in the tangential direction tends to be superdiffuse, i.e.  $\alpha_H > 1$ . b) Bead motion decreases in time after bead adhesion for control case (con, empty triangles), and increases after drug treatment (lat, filled triangles). c) Normalisation removes the effect of changing cell stiffness. Statistically significant changes between drug and control are marked with \*\* for  $p < 0.01$  with Mann-Whitney  $u$ -test. Inset: Cell with bead and tangential direction labelled.

distribution departs from a normal distribution at circa  $|z| = 4$ . As the delay time increases to the plateau time, the increment distribution from control cells develops broad tails, while the actin-disrupted cells exhibit a smaller increase. This is likely due to the reduced contribution of active processes within the disrupted cytoskeleton of the drug treated cells. At both the plateau time and longer timescales, the break from normal distribution occurs around  $|z| = 3$ , indicating a systematic increase in large displacements relative to the shortest timescale.

To further characterise the non-equilibrium component of the bead motion, the long-time superdiffuse motion labelled region iii) in Fig. 1e was analysed with least squares fitting (Eq. (6)) to the MSD in the tangential direction. This latter direction was chosen as it is more comparable to previous particle tracking experiments [20–22]. The pseudo-diffusion coefficients are shown in Fig. 6. Inspection of the power-law exponent reveals that the motion over timescales of tens of seconds tends to be super-diffuse, i.e.  $\alpha_H > 1$ . This indicates correlated motion on long timescales, which would not be possible if the system were at thermal equilibrium. Previous passive microrheology studies of cells have attributed this superdiffusion to cytoskeletal reorganisation [20].

Changes to long-time pseudo-diffusion parameters show a significant decrease in  $D_H$  for the control cells, which means the internal force generation causes a lower strain rate within the cell. The reverse is true for the actin-disrupted cells, with a greater strain rate after drug treatment. However, this is not the whole picture. When the MSD is normalised by the geometric stiffness of the cell, the change in normalised pseudo-diffusion coefficient,  $D_{CH}$ , shows the opposite trend. In other words, the strain rate of

control cells decreases because of the increase in the stiffness of the cell, and not because of a decrease in cytoskeletal rearrangement. Conversely in the actin-disrupted cells, the strain rate increases because the cell is softer while the cytoskeletal activity is reduced. This is indicative of the activity of molecular motors increasing with time after bead adhesion in the control case, while the drug-treated cells do not have the same ability to coordinate their cytoskeletal activity due to the disruptive action of the drug.

## 5. Discussion

In this work, we have demonstrated the effectiveness of a non-invasive passive microrheology technique for probing different processes at different timescales of living cells. We have presented a quantitative analysis of the time-dependent bead MSD and increment distribution based on an analogy to the well-established analytical framework used for optical trapping microrheology. Our approach enables quantitative analysis of cellular interactions with a functionalised surface, and the tracking of a cell's viscosity and elasticity over several hours.

We have observed cells stiffening after bead adhesion and softening after treatment with an actin depolymerising drug, while the viscosity probed remained invariant. The beads were functionalised with streptavidin as it is known to bind with high affinity to integrin receptors [35,36]. Activation of integrin receptors results in the formation of connections between these receptors and the actin cytoskeleton, resulting in reorganisation of the actin cytoskeleton [37]. This may increase cell stiffness due to the formation of actomyosin stress fibres. In drug treated cells, the actin cytoskeleton is disrupted and such integrin mediated cell stiffening could not occur.

Focal complex formation, including actin recruitment, after integrin binding offers one plausible mechanism by which the binding of a bead could cause cells to stiffen [37,38]. This correlates with the observed increase of the geometric stiffness after the binding of a bead to the cell. No previous study, to our knowledge, has reported changes in mechanical properties during the maturation of focal adhesions.

The softening of the cell observed after addition of Latrunculin B represents a partial loss of the contribution of actin to the stiffness of the cell. Actin is primarily located within the actin cortex, visible in Fig. 3, which is known to be the main determinant of the cortical elasticity.

Interpretation of results through the framework of passive microrheology assumes that the cell-bead system is in thermal equilibrium, meaning the MSD is equivalent to the shear creep compliance according to the fluctuation-dissipation theorem. Living cells are clearly far from equilibrium, however previous studies of the microrheology of active actin-myosin gels [39] and of living cells [33] demonstrate that for time scales less than 1s (i.e.: regions i and ii on Fig. 1e), thermally excited motion dominates and the generalised Stokes-Einstein relation (Eq. (3)) is still applicable. This is reflected in the increment distributions which are near-Gaussian for short lag times and broad tailed for longer lag times.

The mechanical properties of the cytoskeleton can be measured using active microrheology with extracellular probes, giving rise to the soft glassy rheology model [24]. Similar power-law scaling was found using passive microrheology by tracking endogenous intracellular probes [33]. These results validate the interpretation of our passive microrheology using extracellular probes to test the mechanical properties of the cytoskeleton.

Prior passive microrheology with extracellular probes have suggested cytoskeletal rearrangement as the cause of superdiffuse motion at long times (MSD power-law exponent  $\alpha_H > 1$ ), as also reported in this work. However, studies did not report measurements of displacements over timescales less than a second [21,22,40].

An optical trap can be used to control bead binding to cells, allowing us probe the mechanical properties of the binding site at time scales of less than a millisecond, limited by the frame rate of the camera, while tighter binding of the bead to the cell would result in motion being below the detection limit on millisecond timescales. Passive microrheology can be used to track the mechanical properties of the cytoskeleton unperturbed by rejuvenation effects caused by deformation under applied forces [20,41]; this, however, limits study to the linear viscoelastic response regime, precluding study of behaviours such as visco-plastic deformation or stress-dependent stiffening.

The viscosity inferred from Eq. (5) was found to be constant for all measurements. Invariant viscosity of integrin complexes has been reported before using an active microrheology method [23], but this is the first time it has been reported using a passive method. We also observe that although disrupting the actin cytoskeleton with Latrunculin B causes a significant reduction in the geometric stiffness, there is still no significant change to the viscosity. Thus the viscosity probed is independent of cytoskeletal changes induced in our experiments by the addition of Latrunculin B.

At time-scales around a second, the cell behaves as a soft glassy material exhibiting weak power-law scaling; at these time-scales the microrheology may only probe longitudinal modes of the cytoskeleton rather than shear modes of the cytoskeleton and cytosol [42]. This can be understood by considering the behaviour of the cytosol when the cytoskeleton is displaced through it: at sufficiently low frequencies, the cytosol is able to drain freely, and its viscosity will no longer affect deformations of the cytoskeleton.

At longer time-scales, the microrheology probes the active strain fluctuations of the cell [22,33], which are a result of cytoskeletal rearrangements [21,41]. Thus the MSDs at lag-times of greater than 10s reported here are higher than if all motion were thermally excited. These slow strain fluctuations are shown to decrease in magnitude in parallel to the stiffening of the cell, while the power law exponent decreases in time after bead adhesion in almost all cases.

## 6. Conclusion

In this work we have presented a quantitative analysis of the changes in mechanical properties of living cells by means of non-invasive passive microrheology measurements. These were performed for up to two hours after a microsphere was bound to the outside of a cell. This is, to our knowledge, the first time that a microrheological technique has been used to observe cytoskeletal changes over such extended time scale, and the first report of cell stiffness changes induced by integrin binding.

The pseudo-Brownian motion of the probe particle was monitored over an experimental time window ranging from  $10^{-3}$  to  $10^3$  s and the MSD was interpreted through an analytical framework based on a Generalised Langevin Equation, which has been validated in literature in the case of microrheology with optical tweezers. The approach used in this work allows us to probe the high frequency mechanical properties of cells without the need of external forces. Non-drug treated control cells were seen to become stiffer over tens of minutes, which is interpreted as a result of the cytoskeletal reorganisation induced by integrin binding. This stiffening is prevented by treating the cells with Latrunculin B, an actin depolymeriser. This interpretation is supported by literature on streptavidin-integrin binding [35], and the interplay between integrins and the actin cytoskeleton [37].

Notably, our results are in agreement with previous microrheology studies of live cells. In particular, we report (i) constant viscosity during normal cell functions, (ii) a weak power-law scaling in the elastic modulus, and (iii) active fluctuations at long time scales.

In addition we identify time-scales where the thermal fluctuations of the cell dominates and those where the dynamics of the cell are governed by actively (driven) processes, how these regime change are interpreted and discussed.

## 7. Materials and methods

Hela S3 (ATCC CCL-2) cells were grown in Dulbecco's Modified Eagle Medium, supplemented with 10% (v/v) Fetal Bovine Serum (Merck: F9665), 1% (v/v) L-glutamine (Merck: G7513), 1% (v/v) Penicillin-Streptomycin solution (Merck: P0781) and 1% (v/v) Non-essential Amino Acid Solution (Gibco:11140-050); these were grown in a T75 flask using the same protocols as for adherent cells. A portion of the cells were adhered to the flask at any time, and these cells were used for experiments while the cells which remained in suspension were used to continue the cell line. The HeLa S3 cell line was chosen as they adhere to glass coverslips but remain rounded (as shown in Fig. 3), allowing the bead to be placed where the cell surface is normal to the imaging plane, shown in Fig. 1b. Adhesion to the coverslip is essential to prevent Brownian motion of the whole cell during the experiment.

Confocal microscopy (Fig. 3) was performed on a Zeiss LSM900 microscope with Airyscan 2 detector, using a 20x 0.6NA objective lens. Cells were seeded 24 h in advance at a density of  $10^5$  cells per 25mm coverslip coated with PLL (Merck, P04707) as described by the manufacturer to promote cell adhesion, fixed in 4% formaldehyde solution (Merck, 1.00496), permeabilised with 0.1% Triton X-100 and stained with Rhodamine Phalloidin (ThermoFisher Scientific R415) and Hoechst 33342 (ThermoFisher Scientific, H3570) for actin and DNA respectively. This method was based on a protocol by Mitchison et al. [43]. To image the effects of Latrunculin B (Merck, L5288), the cells were incubated with the drug at 1mM in serum-free DMEM for 10 min before fixing.

Before microrheology experiments,  $10^4$  cells per well were seeded into an 8 well cavity microslide (Ibidi, Germany, 80841) with 500  $\mu$ L of growth media as above. Cells were incubated overnight at 37°C with 5% CO<sub>2</sub>, and 2 h before experiments the media was changed for 200  $\mu$ L of serum-free Minimum Essential Medium Eagle (Merck: M2279) supplemented as for the growth media (with the exception of FBS) and 5 $\mu$ g Calcein-AM (ThermoFisher, USA, C3099) for fluorescent viability imaging.

Optical trapping and microrheology experiments were performed on a custom microscope set up as follows: a 3W 1064nm ND:YAG was coupled into the back focal plane of an inverted microscope (Nikon, Japan). A 1.3NA, 100x oil immersion objective (Nikon, Japan) is used to focus the beam into the sample, which was mounted on a motorised XY stage (MS-2000, ASI Instruments). The optical trap was used to position polystyrene beads (Spherotech, USA) relative to individual cells. Imaging was performed in transmission using the same objective to form an image on an sCMOS camera (QImaging, Canada).

The image acquisition was controlled using  $\mu$ Manager [44]. Data collection for each microrheology measurement was as follows: first, a full field of view image is collected, before starting a sequence acquisition with reduced field of view (see Fig. 1a iv for example), allowing frame rates over 1,000 frames per second. To find the bead position in each image, first the background is removed by subtracting a value (manually chosen before the acquisition) from every pixel (pixel values below the threshold become 0, not negative), and the image centroid is calculated in Java using code adapted from the ImageJ source code [45].

A typical video measurement comprises of 1 million images over around 9 min. The centroid co-ordinates from every image are stored during acquisition, for example Fig. 1c. The image and

metadata for only every thousandth image are retained for future reference thus reducing storage and memory footprint. After the sequence acquisition, the field of view on the camera is reset and a second full field of view image is collected. Finally, data is saved to disk for later analysis.

## Declaration of Competing Interest

The authors declare that they have no known competing financial interests or personal relationships that could have appeared to influence the work reported in this paper.

## Acknowledgments

This work was supported by the Engineering and Physical Sciences Research Council (EPSRC) under grants EP/S0214334/1, EP/L016052/1, EP/R035067/1, EP/R035563/1, EP/R035156/1 "Experiencing the micro-world: a cell's perspective", the Oxford and Nottingham Biomedical Imaging (ONBI) CDT and the University of Nottingham. The authors thank the Nanoscale and Microscale Research Centre (nmRC) for providing access to instrumentation for confocal microscopy experiments.

## Supplementary material

Supplementary material associated with this article can be found, in the online version, at doi:10.1016/j.actbio.2023.04.039.

## References

- [1] M. Brandão, A. Fontes, M. Barjas-Castro, L. Barbosa, F. Costa, C. Cesar, S. Saad, Optical tweezers for measuring red blood cell elasticity: application to the study of drug response in sickle cell disease, *Eur. J. Haematol.* 70 (2003) 207–211.
- [2] J. Guck, S. Schinkinger, B. Lincoln, F. Wottawah, S. Ebert, M. Romeyke, D. Lenz, H.M. Erickson, R. Ananthakrishnan, D. Mitchell, J. Käs, S. Ulvick, C. Bilby, Optical deformability as an inherent cell marker for testing malignant transformation and metastatic competence, *BioPhys. J.* 88 (2005) 3689–3698.
- [3] F.-S. Quan, K.S. Kim, Medical applications of the intrinsic mechanical properties of single cells, *Acta Biochim. BioPhys. Sin.* 48 (2016) 865–871.
- [4] J. Mitchison, M. Swann, The mechanical properties of the cell surface, *J. Exp. Biol.* 31 (1954) 443–460.
- [5] J. Guck, R. Ananthakrishnan, H. Mahmood, T.J. Moon, C.C. Cunningham, J. Käs, The optical stretcher: a novel laser tool to micromanipulate cells, *BioPhys. J.* 81 (2001) 767–784.
- [6] F. Pérez-Cota, R.J. Smith, E. Moradi, L. Marques, K.F. Webb, M. Clark, High resolution 3D imaging of living cells with sub-optical wavelength phonons, *Brillouin, Sci. Rep.* 6 (2016).
- [7] G. Antonacci, T. Beck, A. Bilenca, J. Czarske, K. Elsayad, J. Guck, K. Kim, B. Krug, F. Palombo, R. Prevedel, et al., Recent progress and current opinions in Brillouin microscopy for life science applications, *BioPhys. Rev.* 12 (2020) 615–624.
- [8] J.-T. Hang, Y. Kang, G.-K. Xu, H. Gao, A hierarchical cellular structural model to unravel the universal power-law rheological behavior of living cells, *Nat. Commun.* 12 (2021) 6067.
- [9] D. Stamenovic, D.E. Ingber, Models of cytoskeletal mechanics of adherent cells, *Biomech. Model. Mechanobiol.* 1 (2002) 95–108.
- [10] J.-T. Hang, G.-K. Xu, H. Gao, Frequency-dependent transition in power-law rheological behavior of living cells, *Sci. Adv.* 8 (2022) eabn6093.
- [11] T.G. Mason, K. Ganesan, J.H. van Zanten, D. Wirtz, S.C. Kuo, Particle tracking microrheology of complex fluids, *Phys. Rev. Lett.* 79 (1997) 3282.
- [12] T.A. Waigh, Microrheology of complex fluids, *Rep. Prog. Phys.* 68 (2005) 685.
- [13] T.A. Waigh, Advances in the microrheology of complex fluids, *Rep. Prog. Phys.* 79 (2016) 074601.
- [14] T.G. Mason, D.A. Weitz, Optical measurements of frequency-dependent linear viscoelastic moduli of complex fluids, *Phys. Rev. Lett.* 74 (1995) 1250.
- [15] J. Xu, V. Viasnoff, D. Wirtz, Compliance of actin filament networks measured by particle-tracking microrheology and diffusing wave spectroscopy, *Rheol. Acta* 37 (1998) 387–398.
- [16] J.S. Lee, P. Panorchan, C.M. Hale, S.B. Khatau, T.P. Kole, Y. Tseng, D. Wirtz, Ballistic intracellular nanorheology reveals rock-hard cytoplasmic stiffening response to fluid flow, *J. Cell Sci.* 119 (2006) 1760–1768.
- [17] B.D. Matthews, D.R. Overby, F.J. Alenghat, J. Karavitis, Y. Numaguchi, P.G. Allen, D.E. Ingber, Mechanical properties of individual focal adhesions probed with a magnetic microneedle, *Biochem. Biophys. Res. Commun.* 313 (2004) 758–764.
- [18] G. Lenormand, P. Bursac, J.P. Butler, J.J. Fredberg, Out-of-equilibrium dynamics in the cytoskeleton of the living cell, *Phys. Rev. E* 76 (2007) 041901.

- [19] A.R. Bausch, U. Hellerer, M. Essler, M. Aepfelbacher, E. Sackmann, Rapid stiffening of integrin receptor-actin linkages in endothelial cells stimulated with thrombin: a magnetic bead microrheology study, *BioPhys. J.* 80 (2001) 2649–2657.
- [20] P. Bursac, G. Lenormand, B. Fabry, M. Oliver, D.A. Weitz, V. Viasnoff, J.P. Butler, J.J. Fredberg, Cytoskeletal remodelling and slow dynamics in the living cell, *Nat. Mater.* 4 (2005) 557–561.
- [21] P. Bursac, B. Fabry, X. Trepate, G. Lenormand, J.P. Butler, N. Wang, J.J. Fredberg, S.S. An, Cytoskeleton dynamics: fluctuations within the network, *Biochem. Biophys. Res. Commun.* 355 (2007) 324–330.
- [22] S.S. An, B. Fabry, M. Mellema, P. Bursac, W.T. Gerthoffer, U.S. Kayyali, M. Gaestel, S.A. Shore, J.J. Fredberg, Role of heat shock protein 27 in cytoskeletal remodeling of the airway smooth muscle cell, *J. Appl. Physiol.* 96 (2004) 1701–1713.
- [23] A.R. Bausch, F. Ziemann, A.A. Boulbitch, K. Jacobson, E. Sackmann, Local measurements of viscoelastic parameters of adherent cell surfaces by magnetic bead microrheometry, *BioPhys. J.* 75 (1998) 2038–2049.
- [24] B. Fabry, G.N. Maksym, J.P. Butler, M. Glogauer, D. Navajas, J.J. Fredberg, Scaling the microrheology of living cells, *Phys. Rev. Lett.* 87 (2001) 148102.
- [25] R.L. Warren, M. Tassieri, X. Li, A. Glidle, D.J. Paterson, A. Carlsson, J.M. Cooper, Rheology at the micro-scale: new tools for bio-analysis, in: *Opt. Meth. Insp. Charact. Imaging Biomater.*, 8792, 2013, p. 879214.
- [26] M. Tassieri, R. Evans, R.L. Warren, N.J. Bailey, J.M. Cooper, Microrheology with optical tweezers: data analysis, *New J. Phys.* 14 (2012) 115032.
- [27] H. Zhang, K.K. Liu, Optical tweezers for single cells, *J. R. Soc. Interface* 5 (2008) 671–690.
- [28] N. Tarantino, J.-Y. Tinevez, E.F. Crowell, B. Boisson, R. Henriques, M. Mhlanga, F. Agou, A. Israël, E. Laplantine, TNF and IL-1 exhibit distinct ubiquitin requirements for inducing NEMO–IKK supramolecular structures, *J. Cell Bio.* 204 (2014) 231–245.
- [29] R. Evans, M. Tassieri, D. Auhl, T.A. Waigh, Direct conversion of rheological compliance measurements into storage and loss moduli, *Phys. Rev. E* 80 (2009) 012501.
- [30] M.G. Smith, G.M. Gibson, M. Tassieri, i-RheoFT: Fourier transforming sampled functions without artefacts, *Sci. Rep.* 11 (2021) 1–12.
- [31] M. Tassieri, Microrheology with optical tweezers: peaks & troughs, *Curr. Opin. Colloid Interface Sci.* 43 (2019) 39–51, doi:10.1016/j.cocis.2019.02.006. <http://www.sciencedirect.com/science/article/pii/S1359029418301316>
- [32] M. Tassieri, G.M. Gibson, R. Evans, A.M. Yao, R. Warren, M.J. Padgett, J.M. Cooper, Measuring storage and loss moduli using optical tweezers: Broad-band microrheology, *Phys. Rev. E* 81 (2010) 026308.
- [33] A.W. Lau, B.D. Hoffman, A. Davies, J.C. Crocker, T.C. Lubensky, Microrheology, stress fluctuations, and active behavior of living cells, *Phys. Rev. Lett.* 91 (2003) 198101.
- [34] E.R. Weeks, D. Weitz, Properties of cage rearrangements observed near the colloidal glass transition, *Phys. Rev. Lett.* 89 (2002) 095704.
- [35] R. Alon, E. Bayer, M. Wilchek, Cell adhesion to streptavidin via RGD-dependent integrins, *Eur. J. Cell Bio.* 60 (1993) 1–11.
- [36] C. Jurchenko, Y. Chang, Y. Narui, Y. Zhang, K.S. Salaita, Integrin-generated forces lead to streptavidin-biotin unbinding in cellular adhesions, *BioPhys. J.* 106 (2014) 1436–1446.
- [37] S. Wiesner, K. Legate, R. Fässler, Integrin-actin interactions, *Cell. Mol. Life Sci.* 62 (2005) 1081–1099.
- [38] O. Adamczyk, Z. Baster, M. Szczypior, Z. Rajfur, Substrate stiffness mediates formation of novel cytoskeletal structures in fibroblasts during cell–microspheres interaction, *Int. J. Mol. Sci.* 22 (2021) 960.
- [39] D. Mizuno, D. Head, F. MacKintosh, C. Schmidt, Active and passive microrheology in equilibrium and nonequilibrium systems, *Macromol.* 41 (2008) 7194–7202.
- [40] G. Lenormand, E. Millet, C.Y. Park, C.C. Hardin, J.P. Butler, N.I. Moldovan, J.J. Fredberg, Dynamics of the cytoskeleton: How much does water matter? *Phys. Rev. E* 83 (2011) 061918.
- [41] X. Trepate, L. Deng, S.S. An, D. Navajas, D.J. Tschumperlin, W.T. Gerthoffer, J.P. Butler, J.J. Fredberg, Universal phys. responses to stretch in the living cell, *Nat.* 447 (2007) 592–595.
- [42] A.J. Levine, T. Lubensky, One- and two-particle microrheology, *Phys. Rev. Lett.* 85 (2000) 1774.
- [43] L. Cramer, A. Desai, Fluorescence procedures for the actin and tubulin cytoskeleton in fixed cells, 2012. [https://mitchison.hms.harvard.edu/files/mitchisonlab/files/fluorescence\\_procedures\\_for\\_the\\_actin\\_and\\_tubulin\\_cytoskeleton\\_in\\_fixed\\_cells.pdf](https://mitchison.hms.harvard.edu/files/mitchisonlab/files/fluorescence_procedures_for_the_actin_and_tubulin_cytoskeleton_in_fixed_cells.pdf). Accessed 2022-12-15.
- [44] A. Edelstein, N. Amodaj, K. Hoover, R. Vale, N. Stuurman, Computer control of microscopes using µ manager, *Curr. Protoc. Mol. Bio.* 92 (2010) 14–20.
- [45] C.A. Schneider, W.S. Rasband, K.W. Eliceiri, NIH image to imagej: 25 years of image analysis, *Nat. Meth.* 9 (2012) 671–675.